Rev.Adv.Mater.Sci. 12 (2006) 182-188

NANOHETEROINTERFACE WAVE FUNCTION PENETRATION LENGTH PHOTONIC CHARACTERISATION

E. A. Anagnostakis

Nanodevice Physics Forum, 72 Cyprus Str., GR 112 57 Athens, Greece

Received: November 12, 2005

Abstract. The persistent photoenhancement (PPE) of the mobility of the two-dimensional electron gas (2DEG) dwelling within a typical functional semiconductor nanoheterointerface (NHI) is processed to yield the energetic separation between the fundamental and first excited conduction subband of the NHI quantum well (QW). Upon that, a finite difference method NHI wave function (WF) engineering is employed to determine the crucial optoelectronic parameter of NHI WF penetration length (into the QW energetic barrier layer) tantamount to the 2DEG mobility behavior, a satisfactory agreement with alternatively obtained values for this parameter being reached.

1. INTRODUCTION.

The investigation of semiconductor heterointerfaces is a prominent subject of ongoing research in view of the crucial importance which they possess for the tunability of numerous optoelectronic nanodevices [1–7]. Celebrated pioneering functional nanoheterostructures of the kind have been the Bloch oscillator [8,9], the resonant tunnelling double heterodiode [10], the hot electron tunnelling transistor [11], and the revolutionary quantum cascade LASER [12,13]. In particular, monitoring of the photoconductive response of NHI structures is regularly utilised as a powerful non-destructive experimental tool [14– 20].

In the present paper, the persistent photoenhancement (PPE) [21-23] of the mobility of the two-dimensional electron gas (2DEG) dwelling within a typical functional semiconductor nanoheterointerface (NHI) is processed to yield the energetic separation between the fundamental and first excited conduction subband of the NHI quantum well (QW). By virtue of this, a simulative model rectangular QW is seeked for; thus providing an effective spatial width for the actual NHI QW hosting the 2DEG wave function (WF), along with an estimation for the crucial optoelectronic parametre of the NHI WF penetration length into the QW energetic barrier layer – tantamount to the 2DEG mobility behaviour.

Corresponding author: E. A. Anagnostakis, e-mail: emmanagn@otenet.gr

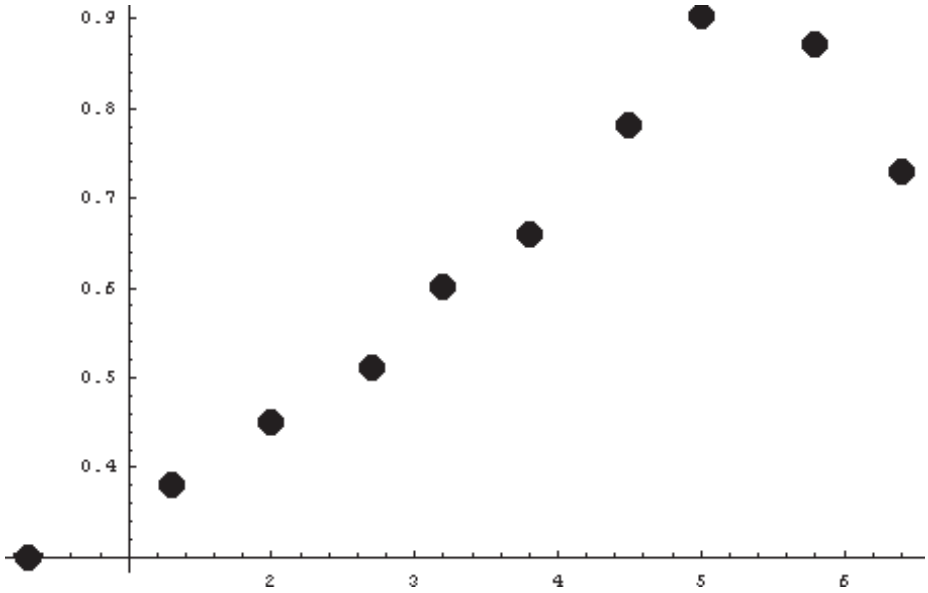

Fig. 1. Reduced PPE $\Delta\mu/\mu_0$ in the NHI 2DEG mobility μ versus the decimal logarithm $\log(\delta/\delta_0)$ of the reduced incoming cumulative photon dose.

The Sturm–Liouville eigenvalue system comprising the quantum mechanical Schrödinger differential equation for the NHI WF and the appropriate asymptotic boundary conditions is treated by a finite difference method after the employment of an independent variable transformation restricting the integration domain to a universal dimensionless interval. The handling of the problem evolves into the numerical calculation of the eigenvectors and respective eigenvalues of a specific tridiagonal matrix hosting the three successions of coefficients appearing in the kind of finite difference equations selected to convergingly approach the initial Sturm–Liouville differential equation.

2. 2DEG MOBILITY PHOTOENHANCEMENT

The NHI probed is formulated within typical molecular beam epitaxy (MBE)–grown functional semiconductor structures, each consisting of an upper, wide band gap, N-type (Si donor – doped at a concentration of the order of $1\cdot10^{17}$ cm^{-3}) $Al_xGa_{1-x}As$ ($x\approx0.3$) epitaxial layer with a thickness of the order of 2 μm grown upon a lower, narrower band gap, relatively P-type-like, non-intentionally doped (NID) GaAs epitaxial layer with a thickness of about 100 nm mounted on top of a semi-insulating (SI) GaAs substrate. The NHI of each device comprises the ionised donor depletion zone on the upper epilayer side and the 2DEG QW hosted within the lower epilayer.

Each device, subjected to the persistent photoconductivity (PP) experimental conditions [24,25] by the provision of successive regulated photon doses evolving within six orders of magnitude, is illuminated from the upper epitaxial layer side with normally incident light filtered to photon energies greater than the band gap of each semiconductor and, thus, capable of producing interband transitions. The device is being kept at a constant temperature of around 4K and a magnetic field of about 0.5 T is being applied within an automated Hall apparatus for the pertinent van der Pauw technique measuring the persistent photoenhancement (PPE) of both the NHI 2DEG population and the NHI 2DEG mobility.

Fig.1 presents, for a representative, such device treated among other in our previous publication [26], the reduced (with respect to the unperturbed dark value μ_0) PPE $\Delta\mu/\mu_0$ in the NHI 2DEG mobility μ versus the decimal logarithm $\log(\delta/\delta_0)$ of the reduced (with respect to a device-wise meaningful reference value δ_0) incoming cumulative photon dose δ. The illumination – induced 2DEG mobility enhancement $\Delta\mu$ is increasing up to a critical cumulative photon dose value Δ such that $\log(\Delta/\delta_0) = 4.86$, then drop-

ping; a negative differential mobility (NDM) regime being thus monitored and recorded.

For interpreting this NDM regime evident reproducibly for all probed devices in the NHI 2DEG mobility PPE experimental curve, we come to consider that, as the cumulative photon dose δ absorbed by the device increases, the conduction electrons confined within the NHI QW (and expected to be occupying solely the QW fundamental conduction subband in the electric quantum limit of operation of the device at 4K) evolve to higher numbers (due to the augmentation of the initial dark concentration of theirs by the rising persistent photoelectron density). And, from some critical total photon dose onwards, the capacity of the QW fundamental conduction subband gets saturated, thus triggering off the onset of the occupancy of the first excited NHI QW conduction subband.

As regards the relation between the mobilities μ_0 and μ_1 of a conduction electron hosted by the fundamental and first excited QW subband, respectively, experimental evidence concerning the electronic charge build-up in GaAs – related microdevices [27,28] allows the assumption that the former is greater than the latter: $\mu_0 > \mu_1$. This comes well in compliance with realising that the fundamental subband wave function in a generic NHI QW tends to peak around the QW centre, as contrasted to the first excited subband wave function exhibiting maxima of the probability of electron dwelling in the proximity of the NHI QW potential energy walls [29] (neighbouring to the NHI roughness and ionised donor depletion zone) and, thus, being more vulnerable to mobility–limiting mechanisms.

Therefore, the ignition of the occupation of the NHI QW first excited conduction subband is linked with a drop in the average 2DEG mobility μ, now expected to lie between the ordered values μ_0 and μ_1, whilst prior to the saturation of the capacity of the fundamental subband μ had simply to be equal to the value μ_0 for fundamental conduction electrons. This drop should be continuous, following the accumulation of ever new persistent photoelectrons on the NHI QW excited subband.

The above reasoning is consistent with the experimentally observed NDM feature $d\mu/d\delta < 0$ in the NHI 2DEG average mobility μ PPE $\Delta\mu$ versus incoming cumulative photon dose δ curve. It, furthermore, allows for the NHI QW fundamental conduction subband capacity Z (in electrons per cm^2 of area normal to the QW bottom) to be experimentally obtained as the initial dark areal concentration ζ_0 plus the value of 2DEG sheet density PPE $\Delta\zeta$ corresponding to the critical cumulative photon dose Δ, after which the NDM regime starts establishing itself in the 2DEG mobility PPE versus photon dose curve. In this fashion, out of the $\Delta\zeta$ versus $\log(\delta/\delta_0)$ experimental plot for the representative device of publication [26], the capacity Z of the fundamental subband, saturated at $\log(\Delta/\delta_0) = 4.86$, is determined as $1.01 \cdot 10^{12}$ electrons/cm^2.

We proceed by visualising, now, that the onset of the occupancy of the NHI QW first excited subband occurs as soon as the conduction electrons already confined within the QW energetically span the interval $\Delta E = Z/\rho$, with ρ being the well-known two-dimensional density of states (number of accessible energy states per unit energy graduation and per unit area normal to the NHI QW spatial width), given by [30] $\rho = 4\pi m^*/h^2$, for m^* the fundamental conduction electron effective mass valid within the NHI QW semiconductor. Then, having computed ρ for GaAs (with m^* approximated by 0.068 times the free electron rest mass), we obtain for the $0 \leftrightarrow 1$ intersubband energetic separation ΔE the value 35.3 meV.

In the following Section, this NHI intersubband energetic separation will serve as the functional criterion for engineering a simulative rectangular effective QW furnishing a realistic estimation for the spatial extension of the 2DEG envelope wave function; therefore, of both the genuine NHI QW bottom width and the wave function penetration length into the QW potential energy barrier layer.

3. FINITE DIFFERENCE METHOD NHI WF ENGINEERING

With respect to the generic situation of a conductivity electron being hosted by the quantum well (QW) of potential energy profile $U(x)$ against the growth axis coordinate x within a conventional semiconductor nanodevice heterointerface, the pertinent Schrödinger equation, concerning the electron de Boglie time – independent wave function $\psi(x)$ and taking into account the spatial variation $m^*(x)$ of the carrier effective mars, reads:

$$-\frac{d}{dx}\left[\frac{\hbar^2}{2m^*(x)}\frac{d\psi(x)}{dx}\right] + U(x)\psi(x) = E\psi(x), \quad (1)$$

with E being the allowed energy eignevalue conjugate to each physically meaningful wave function ψ (x), solving (1) and vanishing asymptotically at infinities, i.e.

$$\psi(\pm\infty) = 0, \quad (2)$$

and $\hbar$ being Planck's action constant divided by 2π.

The concern for the spatial variation $m(x)$ of the conductivity electron effective mass is intended to be one of the prime ingredients of the computational algorithm undertaken in the present work for a realistic NHI WF engineering, in view of the both theoretically and growth-wise sound fact that the transition from the energetic barrier epitaxial layer to the QW semiconductor slab is not actually abrupt within the NHI: It is, rather, gradually being established (even when not tailored as such) within the span of some (otherwise several) monoatomic layers, through which the meaningful effective mass would be some evolving (linear) intermixing between the individual values pertaining to the distinct semiconductor materials in succession – gradually bridging the starting value identifying the former semiconductor with the ending effective mass value imposed by the latter. Furthermore, it is this realistic effective mass graduation through a monitored NHI that, among other things, renders the proposition of a computational algorithm for a numerical solution of the Schröedinger equation advantageous against a purely analytical attempt towards determining the experimentally accountable wave function and discrete energy eigensystem. Additionally, such a scheme allows for the adequate treatment of any (embedded or simulated) spatial profile of the NHI QW potential energy.

Performing, now, an independent variable transformation, namely,

$$x \equiv \alpha x^{*} Arctunh(\xi) \leftrightarrow \varphi(\xi) \equiv \psi\left[x(\xi)\right], \tag{3}$$

we obtain in place of Eq. (1) the Sturm–Liouville differential equation

$$\frac{d}{d\xi}\left[\mu(\xi)\frac{d\varphi(\xi)}{d\xi}\right] - \upsilon(\xi)\varphi(\xi) + \lambda\sigma(\xi)\varphi(\xi) = 0, \tag{4}$$

under the boundary conditions

$$\varphi(-1) = 0 \;\&\; \varphi(+1) = 0, \tag{5}$$

with functions $\mu(\xi)$,$\upsilon(\xi)$ and $\sigma(\xi)$ in the new dimensionless variable ξ (belonging to the universal interval [-1,+1]) defined as

$$\mu(\xi) \equiv \frac{1}{\alpha}\left(1-\xi^{2}\right)\frac{m_{0}}{m^{*}\left[x(\xi)\right]}, \tag{6}$$

$$\upsilon(\xi) \equiv \frac{2\alpha}{1-\xi^{2}}\frac{U\left[x(\xi)\right]}{E^{*}}, \tag{7}$$

$$\sigma(\xi) \equiv \frac{2\alpha}{1-\xi^{2}}, \tag{8}$$

and dimensionless new, 'reduced energy', eigenvalue λ defined as

$$\lambda = \frac{E}{E^{*}}, \tag{9}$$

where E^{*} denotes a convenient energy scale

$$E^{*} \equiv \frac{\hbar^{2}}{m_{0}x^{*2}} \equiv 1\ eV, \tag{10}$$

rendering the characteristic confinement length x^{*} entering the independent variable transformation (3) after the dimensionless scale factor α equal to 2.76043 Å, m_{o} giving the electron rest mass.

For converting the Sturm–Liouville differential equation concerning the nanoheterointerface two-dimensional electron gas (2DEG) transformed wave function $\varphi(\xi)$ into a linearised system of difference equations, we employ the numerical approximation

$$\frac{d}{d\xi}\left[\mu(\xi)\frac{d\phi(\xi)}{d\xi}\right] \rightarrow \frac{1}{k}\left[\mu_{i+\frac{1}{2}}\left(\frac{\phi_{i+1}-\phi_{i}}{k}\right) - \mu_{i-\frac{1}{2}}\left(\frac{\phi_{i}-\phi_{i-1}}{k}\right)\right], \tag{11}$$

in which the computational (nodal and interstitial, respectively) grid points ξ_{n} (whence $f_{n}\equiv f(\xi_{n})$ with f standing for function φ, μ, υ, and σ, as the case might be) are chosen as

$$\xi_{i} = -1 + ik\,(i = 0,1,2,\ldots,N+1),$$
$$\xi_{i\pm\frac{1}{2}} = \xi_{i} \pm \frac{k}{2}\,(i = 0,1,2,\ldots,N+1), \tag{12}$$

for a uniform grid spacing

$$k = \frac{1-(-1)}{N+1} = \frac{2}{N+1}, \tag{13}$$

and for which the adjoint boundary conditions become, after (5) & (12),

$$\phi_{0} = \phi(\xi_{0}) = \phi(-1) = 0$$
$$\&$$
$$\phi_{N+1} = \phi(\xi_{N+1}) = \phi\left(-1 + (N+1)\frac{2}{N+1}\right) = \phi(+1) = 0. \tag{14}$$

The Schrödinger equation eigenvalue problem is, thus, approximated by the system of difference equations

$$\left\{\alpha_i\phi_{i-1}+\beta_i\phi_i+\gamma_i\phi_{i+1}=-k^2\Lambda\phi_i;\ i=1,2,\ldots,N\right\} \quad (15)$$

or, equivalently, in tridiagonal matrix row form,

$$\left\{\sum_{j=1}^{N}\left\{\left[\alpha_i\delta_{i-1,j}+\beta_i\delta_{i,j}+\gamma_i\delta_{i+1,j}\right]\phi_j\right\}\right.$$
$$\left.=-k^2\Lambda\phi_i;\ i=1,2,\ldots,N\right\} \quad (16)$$

($\delta_{i,j}$ being the Kronecker delta), with the sets of coefficients α_i, β_i, γ_i defined as

$$\alpha\equiv\frac{\mu_{i-\frac{1}{2}}}{\sigma_i},\ \gamma_i\equiv\frac{\mu_{i+\frac{1}{2}}}{\sigma_i},\ \beta_i\equiv$$
$$-\left(\alpha_i+\gamma_i+\frac{k^2v_i}{\sigma_i}\right);\ i=1,2,\ldots,N, \quad (17)$$

and Λ denoting the approximation to the exact reduced energy eigenvalue λ (Eq. (9)), produced by the constructed numerical algorithm and expected to more closely converge to it with increasing number N of computational grid nodal points ξ_i utilised.

The treatment has, therefore, evolved into the matrix eigenvalue problem

$$\left\{\sum_{j=1}^{N}\left\{\Lambda_{i,j}\phi_j\right\}=-k^2\Lambda\phi_i;\ i=1,2,\ldots,N\right\}, \quad (18)$$

with the N-th order square tridiagonal matrix

$$\left\{\left(\Lambda_{i,j};\ j=1,2,\ldots,N\right);\ i=1,2,\ldots,N\right\}$$

defined by

$$\Lambda_{i,j}\equiv\alpha_i\delta_{i-1,j}+\beta_i\delta_{i,j}+\gamma_i\delta_{i+1,j}. \quad (19)$$

Indeed; the opposite of the eignvalues of matrix $\{\Lambda_{i,j}\}$ divided by k^2 give Λ, the approximations to the heterointerface wave function exact reduced energy eigenvalues λ, thus computing (Eq.(9)) the allowed QW 2DEG subband energies $E=\lambda E^*$. Obviously, given that the general Strum–Liouville system (4) may admit an infinite sequence of eigenvalues λ, the finite succession of N eigenvalues Λ for algorithmic matrix $\{\Lambda_{i,j}\}$ provides the numerical approximations to only the N lowest true reduced energy eigenvalues λ, a slightly lessening approximation sufficiency for the last higher order computed eigenvalues being algorithmically probable. On the other hand, the N determined, Strum – Liouville eigenvectors $|\varphi(\xi)\rangle$ conjugate to these numerical eigenvalues Λ unveil through transformation (3) the quantum mechanically allowed wave functions $\psi(x)$ for the 2DEG dwelling within the nanodevice heterointerface QW and underlying the crucial optoelectronic effects exhibited by the generic semiconductor nanostructure. In particular, such a determination of the nanoheterointerface 2DEG wave function may lead to the computation of its entailed penetration length into the nanodevice neighbouring energy barrier layer. Thus, facilitating the prediction of 2DEG mobility behaviour parametrised by the order of wave function excitation and, furthermore, the consideration of quantum mechanical tunnelling transmission probability [19,30,31] for conductivity electrons escaping the heterointerface and travelling through the nanodevice – by virtue of a normal transport mechanism advantageously exploitable, especially at nanoelectronic cryogenic ambient temperatures.

Feeding, now, into the above outlined finite difference method algorithm the $Al_xGa_{1-x}As/GaAs$ probed NHI conduction band discontinuity evaluated as 264 meV after [32], correlating the $Al_xGa_{1-x}As/GaAs$ NHI band edge misfits with compositional indices x, as the QW energetic depth and expressing (in the vicinity of the upper NHI QW boundary) the evolving effective mass $m(x)$ as a linear graduation between the pure $Al_xGa_{1-x}As$ ($x\approx0.3$) and GaAs values (0.0919 and 0.068 times the free electron rest mass, respectively) , we perform iterations with respect to the sought for QW spatial width under the constraint that the simulative rectangular effective QW derived exhibit as fundamental – first excited intersubband energetic separation the closest possible to $\Delta E = 35.3$ meV. This as determined in Section II tantamount to the saturation of the capacity of the actual NHI QW fundamental subband, or – equivalently – the onset of the occupancy of the NHI first excited subband. And – experimentally observably –, with the commencement of the occurrence of NDM regime in the 2DEG mobility PPE $\Delta\mu$ versus incoming cumulative photon dose δ curve. In this fashion, for the representative NHI of [26], the iterative algorithm converges to a QW spatial extension of 186 Å, for which the respective fundamental $\psi_0(x)$ and first excited $\psi_1(x)$ wave- functions along with the adjoint energy eigenvalues E_0 and E_1 are depicted in Fig. 2.

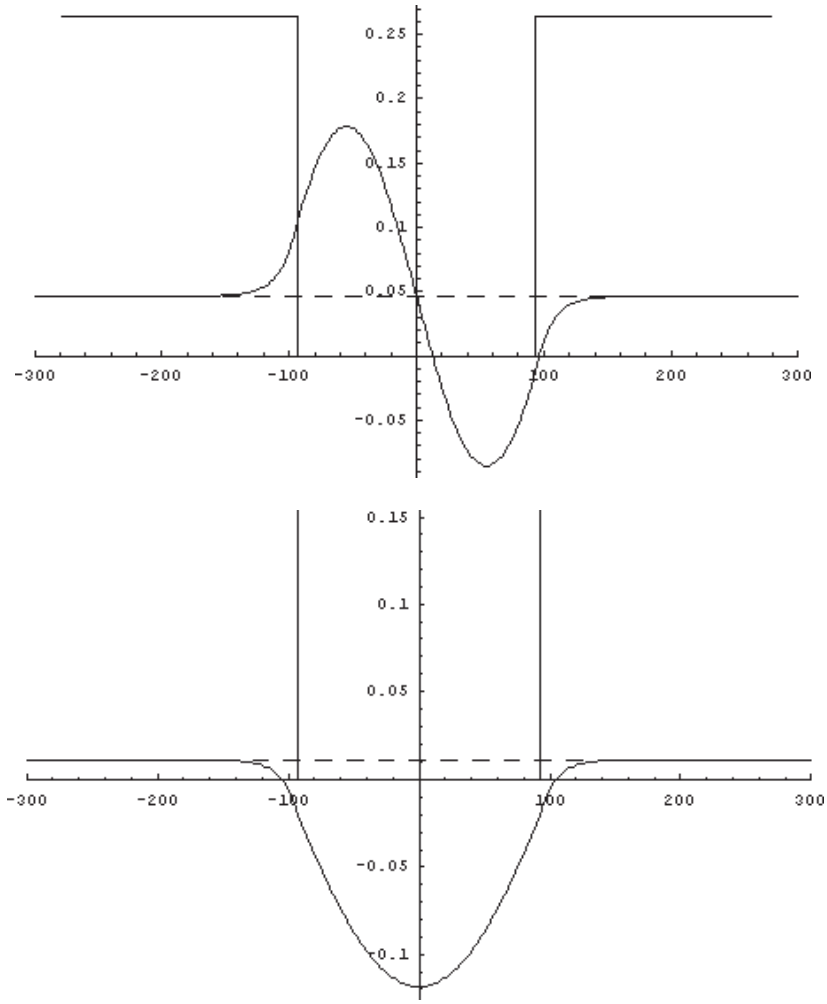

Fig. 2. NHI optimised effective QW hosting the fundamental (lower) and first excited (upper) 2DEG wave-function, with the respective energy eigenvalue marked and the wave-function penetration length traceable.

4. CONCLUSION

A careful investigation of the (fundamental) wave function leakage tail out of the optimised effective NHI QW and into the neighbouring potential energy barrier layer (on the front, illuminated, device side) yields for the crucial optoelectronic parametre of the WF penetration length the value of about 22 Å, permeating the character of 2DEG mobility behaviour versus conduction electron population enhancement in a coherent manner.

On the other hand, the inferred values of NHI characterisation parametres of QW fundamental – first excited intersubband energetic separation, QW spatial width, and 2DEG WF penetration length are understood to be compatible with both the sub- nm scale sharpness of the Si doping profile established by the MBE NHI device growth procedure and the low, electric quantum limit – like, temperature (≈ 4K) of the PPE experiment, allowing for a fine energy resolution between QW subbands of the order of 0.3 meV. The orders of magnitude, furthermore, of the NHI characterisation parametres determined are consistent with the findings [31,33–36] of researches on similar NHIs.

Thus, the employment of the 2DEG mobility PPE evolution against increasing cumulative photon dose absorbed along with the finite difference method iterative algorithm for optimising a simulative effective QW fulfilling the experimentally monitored intersubband energetic separation furnish a reliable NHI characterisation, coming well in compliance with relevant literature.

REFERENCES

[1] J.J. Harris, R. Murray and C. T. Foxon // *Semicond. Sci. Technol.* **8** (1993) 31.

[2] Shengs S. Li, M. Y. Chuang and L. S. Yu // *Semicond. Sci. Technol.* **8** (1993) S406.

[3] L. V. Logansen, V. V. Malov and J. M. Xu // *Semicond. Sci. Technol.* **8** (1993) 568.

[4] C. Juang // *Phys. Rev. B* **44** (1991) 10706.

[5] M. Ya. Asbel // *Phys. Rev. Lett.* **68** (1992) 98.

[6] G. J. Papadopoulos // *J. Phys. A.* **30** (1997) 5497.

[7] F. Capasso and A. Y. Cho // *Surf. Sci.* **299/300** (1994) 878.

[8] R. O. Grondin, W. Porod, J. Ho, D. K. Ferry and G. J. Iafrate // *Superlattices and Microstructures* **1** (1985) 183.

[9] J. N. Churchill and F. E. Holmstrom // *Phys. Lett A* **85** (1981) 453.

[10] T. C. L. G. Sollner, W. D. Goodhue, P. E. Tannenwald, C. D. Parker and D. D. Peck // *Appl. Phys. Lett.* **43** (1983) 588.

[11] N. Yokoyama, K. Imamura, T. Oshima, H. Nishi, S. Muto, K. Kondo and S. Hiyamizu // *Japan. J. Appl. Phys.* **23** (1984) L. 311.

[12] J. Faist, F. Capasso, D. Sivco, D. Sirtori, A. L. Hutchinson S. N. G. Chu and A. Y. Cho // *Science* **264** (1994) 553.

[13] J. Faist, F. Capasso, C. Sirtori, D. L. Sivco, A. L. Hutchinson and A. Y. Cho // *Electron. Lett.* **32** (1996) 560.

[14] Ch. Gauer, J. Scriba, A. Wixforth, J. P. Kotthaus, C. Nguyen, G. Tuttle, J. H. English and H. Kroemer // *Semicond. Sci. Technol.* **8** (1993) S137.

[15] A. B. Henriques and L. C. D. Goncalves // *Semicond. Sci. Technol.* **8** (1993) 585.

[16] H. J. Hovel, *Semiconductors and Semimetals*, *Vol. 11* (Academic Press, New York, 1979).

[17] E. A. Anagnostakis // *Phys. Rev. B* **46** (1992) 7593.

[18] E. A. Anagnostakis // *Phys. Stat. Sol. B* **181** (1994) K15.

[19] Jasprit Singh, *Semiconductor Optoelectronics* (McGraw – Hill, New York, 1995).

[20] G. H. Julien, O. Gauthier – Lafaye, P. Boucaud, S. Sauvage, J. – M. Lourtioz, V. Thierry – Mieg and R. Phanel, *Intersubband Transitions in Quantum Wells: Physics and Devices* (Kluwer Academic Publishers, Boston, 1998).

[21] E. A. Anagnostakis and D. E. Theodorou // *J. Appl. Phys.* **73** (1993) 4550.

[22] S. Brehme // *Semicond. Sci. Technol.* **5** (1990) 983.

[23] E. A. Anagnostakis // *Phys. Stat. Sol. A* **136** (1993) 247.

[24] D. E. Theodorou and E. A. Anagnostakis // *Phys. Rev. B* **44** (1991) 3352.

[25] E. A. Anagnostakis // *Phys. Stat. Sol. A* **126** (1991) 397.

[26] E. A. Anagnostakis and D. E. Theodorou // *Phys. Stat. Sol. B* **188** (1995) 689.

[27] S. Mori and T. Ando // *J. Phys. Soc. Japan* **48** (1980) 865.

[28] H. L. Stormer, A. C. Gossard and W. Wiegmann // *Solid State Commun.* **41** (1982) 707.

[29] M. Jaros, *Physics and Applications of Semiconductor Microstructures* (Oxford University Press, 1989).

[30] C. Weisbuch, *Semiconductors and Semimetals*, *Vol. 24* (Academic Press, New York, 1987).

[31] S. Giugni and T. L. Tansley // *Semicond. Sci. Technol.* **7** (1992) 1113.

[32] B. Vinter // *Surface Sci.* **142** (1984) 452.

[33] T. Ando // *J. Phys. Soc. Japan* **51** (1982) 3893.

[34] R. Fletcher, J. J. Harris and C. T. Foxon // *Semicond. Sci. Technol.* **6** (1991) 54.

[35] K. Miyatsuji, H. Hihara and C. Hamaguchi // *Superlattices and Microstructures* **1**, (1985) 43.

[36] G. Bastard, *Wave Mechanics Applied to Semiconductor Heterostructures* (Les Editions de Physique, Les Ulis Cedex, France, 1988).